Case Studies in Thermal Engineering 43 (2023) 102784

Contents lists available at ScienceDirect

Case Studies in Thermal Engineering

journal homepage: www.elsevier.com/locate/csite

Experimental assessment and modeling of solar air heater with V shape roughness on absorber plate

Rahul Kumar [a], Sujit Kumar Verma [b,g], Naveen Kumar Gupta [b,*], Andrés Z. Mendiburu [c,g], Abhishek Sharma [d], Tabish Alam [e], Sayed M. Eldin [f]

[a] School of Mechanical Engineering, Lovely Professional University, Phagwara, 144411, Punjab, India
[b] Department of Mechanical Engineering, GLA University, Mathura, India
[c] Department of Mechanical Engineering, Federal University of Rio Grande do Sul, Porto Alegre, Brazil
[d] Department of Mechanical Engineering, B.I.T. Sindri, Dhanbad, 828123, Jharkhand, India
[e] CSIR-Central Building Research Institute, Roorkee, India
[f] Center of Research, Faculty of Engineering, Future University in Egypt, New Cairo, 11835, Egypt
[g] International Research Group for Energy Sustainability (IRGES), R. Sarmento Leite 425, Porto Alegre – RS, CEP 90050-170, Brazil

ARTICLE INFO

Keywords:
Triangular
Solar intensity
Heat transfer
Rib roughness
Absorber plate
Coating

ABSTRACT

A roughness of the absorber plate can improve the efficiency of a solar air heater. To boost the efficiency of triangle solar air heaters, this research presents the results of a comparison study between with and without rib roughness on absorber plates. Both use black paint with graphene nanoparticles infused into it, coating an absorber plate. Both numerical and experimental methods have been used to examine the impact of surface roughness on friction factors and heat transport properties. ANSYS 14.5 software module and RNG turbulence, k-ϵ model is used to conduct a three-dimensional simulation and solve the governing equations in the turbulent situation. Based on experimental data, it has been established that smooth plates are more efficient in converting heat into useful work than rough ones, on average, by a factor of 4.82 and 4.46, respectively. The length of the duct in the solar air heater mitigates the temperature gradient seen in the simulation result. The roughness of V-shaped ribs has a far larger effect on the heat transfer and friction factor properties than do variations in relative roughness pitch (P/e) and Reynolds number (Re). Experimental observations supported by modeling and simulation confirms that triangular duct absorber surface roughness provides improved outcome.

1. Introduction

Solar power has the biggest potential among all renewable energy sources since it is sustainable, freely available, and abundant [1]. The availability of reliable and affordable energy is critical to every country's progress. Available solar energy is substantial and can be utilized in versatile ways [2]. One of the most pressing issues facing mankind today is how to harness the sun's power for human needs more effectively to lessen the burden of negative impacts of conventional energy usage. Various solar air heaters can be used with this energy [3]. Conventionally, SAHs are the most economically viable means of solar energy conversion. Common uses for this type of solar thermal system include winter house heating, timber seasoning, grain &crop drying, and space heating [4].

Poongavanam et al. [5] carried out investigation to find whether a shot-blasted V-corrugation absorber plate might rise the heat

* Corresponding author.
E-mail address: naveen.gupta@gla.ac.in (N.K. Gupta).

https://doi.org/10.1016/j.csite.2023.102784
Received 19 October 2022; Received in revised form 15 December 2022; Accepted 26 January 2023
Available online 4 February 2023

transmission of the solar air heater. It was observed that it could; be higher Nusselt than with a regular experimental system, but the friction factor was only slightly higher. Pandey et al. [6] investigated a roughness component of the SAH, NACA profile (0040) ribs' thermohydraulic capacity, and their THPP was found to be 2.53 at a Reynolds number of 6000. Jain and Lanjewar [7] observed that *Nu* is multiplied by 2.3 and the friction factor is multiplied by 3.130 when a V-shaped rib with an asymmetrical gap and staggering rib arrangement is used. To enhance the convective heat transfer rate within SAH, several ribs and coating alternatives are being investigated. So far, in research based on Solar thermal energy, researchers aimed to optimize the gain from solar radiation. In this perspective, the design parameters of solar air heaters, especially the absorber plates, are critical for absorbing maximum power from the sun [8]. The available experiments in the literature are predominantly focused on increasing the absorber's heat transfer surface area. The present study literature survey is divided into two parts: the roughness parameter of the absorber plate and absorber plate nanomaterial coating.

The purpose of this investigation is to examine the differences between absorber plates with smooth and V-shaped roughness. Coatings consist of black paint with graphene infused into it at a rate of 2% in both cases. CFD analysis provides thermohydraulic performance and heat transfer from absorber surface to air. It has a predetermined mass flow rate and adjusts for air temperature and sun intensity. On the other hand, the experimental investigation determines TSAH's thermal efficiency, exergy efficiency, exergy destruction rate, and sustainability index. The is certainly aimed for better understanding of the V-shaped roughness on the TSAH absorber plate.

2. The materials and methods

To explore the impact of a recently developed absorber plate on the performance of TSAH, an experimental system has been designed. Using data from both experimental observations and CFD simulations, a comparative analysis carried out between conventional and modified TSAH. In this investigation, the physical and simulated systems were tested with the use of a TSAH that had several V-shaped ribs with the gap between them and was coated with graphene nano-material. During the CFD analysis and coding, the following assumptions are made.

- Fluid flow is assumed to be stable, incompressible, and turbulent.
- The fluid's characteristics are assumed to be the same through the pipe.
- Atmospheric air is assumed to be the working fluid, with an inlet temperature of 300K.

2.1. Experimental instalation

Experimentation including fabrication, installation and testing carried out at Solar Energy Research Centre at GLA University Mathura. Fig. 1 depicts schematic and experimental design. The dimensions of the triangular section are 1 m, 0.6 m, and 0.52 m, and it has a hydraulic diameter of 0.352 m. The aspect ratio of the triangular work section is 1.15. In experimental observation, it is assumed that the flow of air inside the triangle duct is completely turbulent. With the assistance of an air blower, the air is sucked in from the entry segment at atmospheric conditions.

2.2. Coating preparion

First of all, graphene nanomaterial of 2% concentrations is mixed with a black paint that is painted to the surface of the absorber. A layer of graphite that has been created by a process known as chemical exfoliation is called graphene. The graphene material itself takes the shape of a fluffy, soft, and dark black powder. Fig. 2 displays FESEM images and an EDS analysis of the coating on the absorber plate.

3. Data reduction

3.1. Performance calculations

The starting temperature difference (To) is expected to begin the analytical procedure. $T_o = T_i + \Delta T$

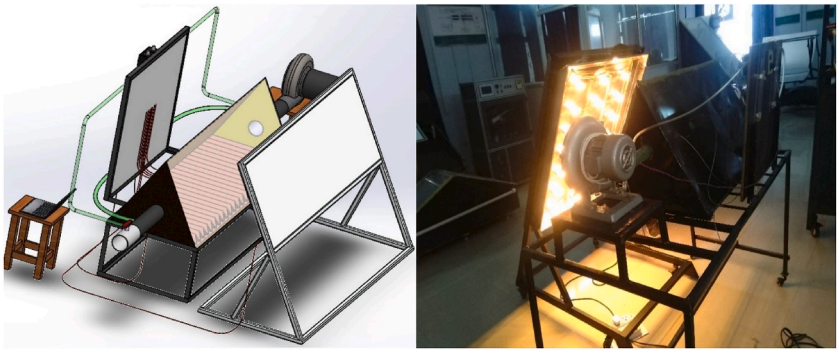

Fig. 1. TSAH Schematic and Experimental arrangement.

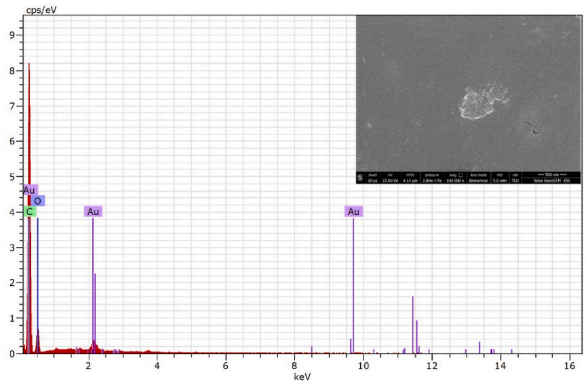

Fig. 2. EDS characterization of the 2% Graphene black paint coating.

An expected average temperature for both absorber plate types is provided by the relationship [9].

$$T_p = \frac{T_0 + T_i}{2} + 10$$

$$h_w = 5.7 + 3.8V$$

The heat loss coefficient of the glazing plate is determined by the average temperature of the absorber surface (Ut), [10].

$$U_t = \left(\frac{N}{\frac{C}{T_p}\left(\frac{(T_p - T_a)}{(N+f)}\right)^e} + \frac{1}{h_w} \right)^{-1} + \frac{\sigma\left(T_p + T_a\right)\left(T_p^{\,2} + T_a^{\,2}\right)}{\frac{1}{\epsilon_p + 0.00591 N h_w} + \left[\frac{2N + f - 1 + 0.133\epsilon_p}{\epsilon_g}\right] - N}$$

$$f = \left(1 + 0.089h_w - 0.01166h_w\epsilon_p\right)\left(1 + 0.07866N\right)$$

$$e = 0.43\left(1 - \frac{100}{T_p}\right)$$

$$C = 520\left[1 - \left(0.000051\beta^2\right)\right] For\ 0^0 < \beta < 70^0$$

$$U_b = \frac{k_i}{t_i}\ [11]$$

$$U_e = U_b\left(\frac{A_e}{A_c}\right)$$

The total heat loss;

$$U_L = U_t + U_b + U_e$$

$$Q_{u1} = A_p\left[I(\tau\alpha) - U_L\left(T_p - T_a\right)\right]$$

The mass flow rate of air can be calculated by the equation [12],

$$\dot{m} = \frac{Q_{u1}}{C_p \Delta T}$$

$$R_e = \frac{\dot{m} D_h}{\mu A_t}$$

$$P_r = \frac{m\dot{C}_p}{k_a}$$

The equation that may be used to calculate the Nusselt number is given below [13],

$$N_u = \frac{3.66 + 0.0668(D_h/L)R_eP_r}{1 + 0.04[(D_h/L)R_eP_r]^{2/3}}$$

The correlation between the Nusselt number and the convection heat transfer coefficient [11,14,15].

$$h = \frac{N_u k_a}{D_H}$$

$$F' = \frac{h}{h + U_L}$$

The following formulas are used to determine the plate efficiency factor [16] and heat removal factor [17];

$$F_R = \frac{\dot{m} C_{pair}}{A_c U_L}\left[1 - exp\left\{\frac{-F' U_L A_p}{\dot{m} C_{pair}}\right\}\right]$$

$$Q_{u2} = F_R A_p [I(\tau\alpha) - U_L(T_o - T_i)]$$

$$\eta_{th} = F_R(\tau\alpha) - \frac{F_R U_L (T_o - T_i)}{I}$$

3.2. Exergy calculations

This is define the net exergy energy rate of the solar air heater [18],

$$E_s = IA_p\left(1 - \frac{T_a}{T_{sun}}\right)$$

Exergy is gained by the collector surface and is denoted as,

$$E_n = IA_p\eta_{th}\eta_c - P_m(1 - \eta_c)$$

$$P_m = \frac{\dot{m}\Delta P}{\rho}$$

$$\eta_c = 1 - \frac{T_a}{T_b}$$

The formula calculates the TSAH's energy efficiency;

$$\eta_{ex} = \frac{E_n}{E_s}$$

Calculations for several forms of exergy destructions look like this [19],

$$E_{opt} = IA_p\eta_{ex}(1 - \tau\alpha)$$

$$E_{abs} = IA_p\tau\alpha\left[\eta_{ex} - \left(1 - \frac{T_a}{T_p}\right)\right]$$

$$E_{env} = U_L A_p\left(T_p - T_a\right)\left(1 - \frac{T_a}{T_p}\right)$$

$$E_{ht} = IA_p\eta_{th}\left[\left(1 - \frac{T_a}{T_b}\right) - \left(1 - \frac{T_a}{T_p}\right)\right]$$

$$E_f = \frac{\dot{m}\Delta P}{\rho T_b}$$

The Sustainability Index (SI) is also a crucial metric for assessing the efficacy of thermal systems that are based on renewable energy sources.

$$SI = \frac{1}{1 - \eta_{ex}}$$

4. Results and discussion

Analytical comparison using computational fluid dynamics (CFD) and experimental evaluation of roughened and smooth absorber plates are carried out here. To ensure that the design that was suggested is an efficient one, CFD model was investigated for validation.

4.1. CFD simulation result

Ansys 14.5 workbench software was used for the numerical simulation to determine the TSAHs' thermal and flow parameters.

Fig. 3 shows the full temperature distribution over the roughened absorber sides of a solar air heater. Due to the reduced quantity of sunlight reaching the absorber plate, TSAH with a tilted absorber plate is less hot than those with horizontal roughened or smooth absorber plates. A section of the input and exit pressure curves is depicted in the duct's input part has a higher pressure than the duct's output section. For this reason, TSAHs with a smooth absorber plate experience less pressure drop than those with a rough absorber plate.

Changing the absorber plate's geometry causes a shift in the relationship between Reynolds and Nusselt numbers. The Nusselt number grows with the Reynolds number for any given configuration of rib roughness. This is because there is now less space between the reattachment point and inter rib zone, which allows for a longer detached flow. The *Nu* for an absorber plate with a roughened V shape and varying rib roughness is significantly higher across the board for Re than one with a smooth surface.

The influence of Reynolds number on Nusselt number and THPP for various absorber face roughened plate layouts is shown in Fig. 4. For a range of rib roughness designs, friction factors drop as Reynolds numbers rise. Reattachment distances and the recirculation zone behind the ribs both decrease with increasing Reynold number. This decrease is brought on by the suppression of the laminar sub-layer that occurs at high Reynolds numbers. For a given Reynolds number, a decrease in the pitch ratio P/D and e/D is observed to increase the THPP. At constant P/D & e/D pitch ratios and increasing Reynolds number, the THPP parameter drops in all situations.

Mesh compatibility for the turbulent flow through the intentionally roughened solar air heater is investigated by conducting a grid-dependency analysis. Three alternative grids, each with a different total number of nodes (184,727, 310,900, and 355,695), are employed in a grid independence test. When expanding from 310,900 to 355,695 cells, the variance in Nusselt number and friction factor is determined to be minimal. Increasing the number of cells above that point will not provide any additional benefit. To facilitate the computation at hand, a grid with 310,900 cells has been decided for the experiment. The computational domain often makes use of non-uniform structured quadrilateral grids. The fine-sizing is set at 40 and the relevance is assumed to be 40.

As the roughness grows, the relative flow rate falls. These patterns of activity are reminiscent of those observed in flows through homogeneously rough microchannels. Turbulence in the flow, created by artificial roughness, increases the heat transmission between the air and the heated wall. The surface roughness was found to have significant effects on the pump's efficiency.

4.2. Experimental result

To compare the heater's thermal efficiency, the investigations were conducted. The sun radiation and air temperature swings occurred throughout the two separate trials. Experiment's average ambient temperatures are 310K.

Fig. 5 shows that the thermal efficiency changes with the amount of sunlight available. Boosting the sun intensity improved the thermal efficiency of the absorber surface in both configurations. Maximum thermal efficiency was reached at a solar intensity of 750 W/m^2, and efficiency dropped down precipitously above that point. A roughened absorber plate has been shown in all studies to have higher average thermal efficiency than alternative TSAHs.

Investigation indicates following observatins: strong absorption of solar radiation, enhanced heat transfer between absorber surfaces and flowing air boost heat gain in TSAH with roughened absorber plate. It has been observed that heat loss was exacerbated by the growing temperature and solar radiation. Similarly, heat loss follows a predictable profile in this study. Fig. 5 displays the shifts in exergy loss components and intensity of solar radiation experienced by roughed plates. The exergy analysis of a SAH relies heavily on the absorber surface temperature. This analysis is essential to grasp the fundamentals of the design and operation of any thermal system. Under all experimental situations, the exergy efficiency tracked the variation in the rate of instantaneous emission or absorption of energy. Exergy efficiency was at a low point at 750 W/m^2 of solar power and rises as intensity from the sun was increased.

The Sustainability Index is a measure of a system's efficiency based on its exergy use. Fig. 6 displays a comparison of roughened and smooth absorber plates in terms of sustainability index vs solar intensity. The temperature and the exergy efficiency function as a whole determines the sustainability index. Both versions of the solar air heater have a intensity magnitude, that is lowest at 780 W/m^2 and increases. For a clearer picture of how the roughened absorber plate in TSAH affects airflow and thermal performance since the temperature of an air current is directly proportional to the amount of solar radiation striking on it, increasing the magnitude of solar

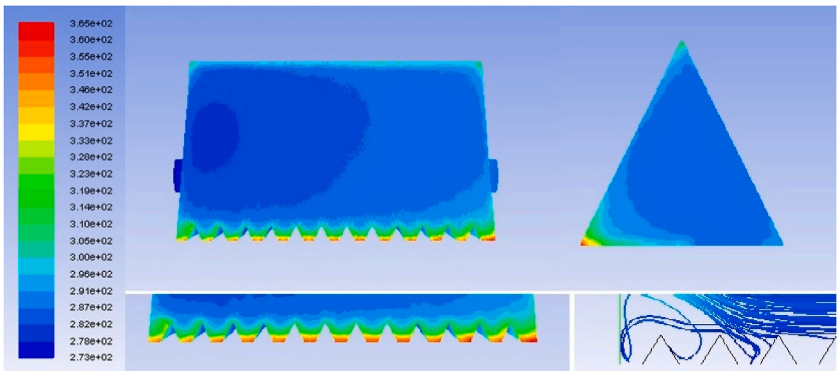

Fig. 3. Roughened absorber plate's roughened temperature contour (TSAH).

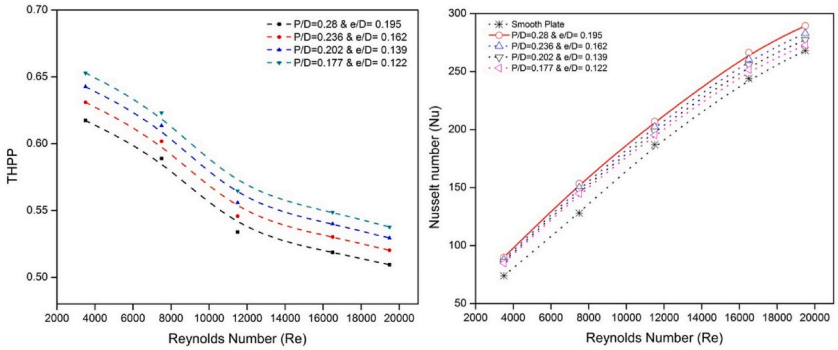

Fig. 4. Variation of the THPP and Nusselt number vs Reynolds number using various roughened plates.

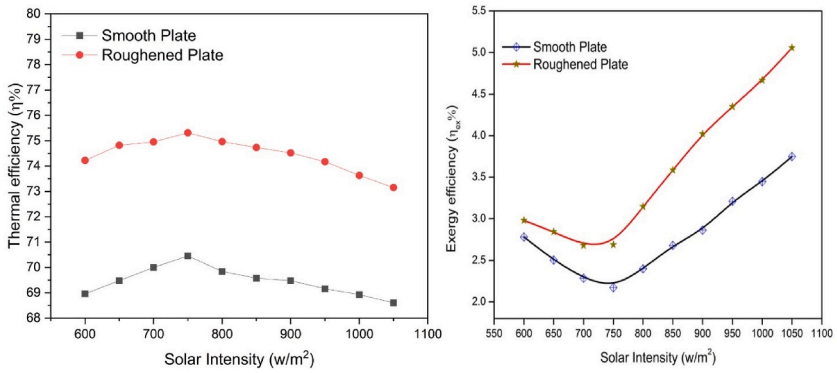

Fig. 5. Solar intensity variation vs thermal efficiency.

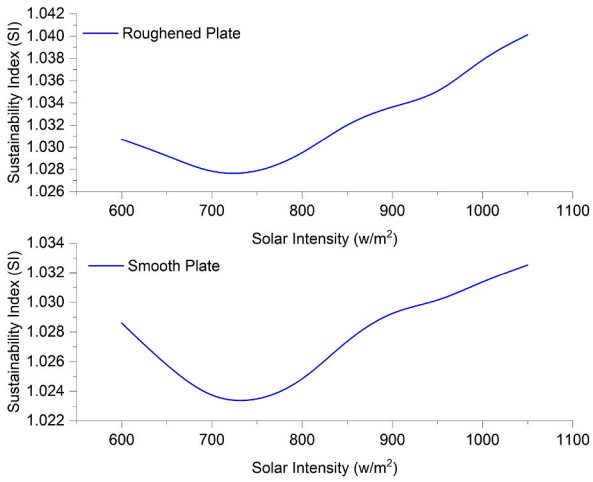

Fig. 6. Comparison of the sustainability index and solar intensity.

radiation causes the air current to heat up to a greater magnitude.

It has been compared between the Nusselt number and friction factor obtained using the Dittus-Boelter equation and the modified Blasius equation, respectively, with the values determined experimentally for a smooth duct. The experimental results verify by the CFD findings. Results from computational fluid dynamics (CFD) and experiments showed that, with an insolation of 750 W/m^2, the heat transfer coefficient is 7.5 W/m$^{2\circ}$C and 7.29 W/m$^{2\circ}$C, respectively. The discrepancy between CFD and experimental results was found to be between 1.5% and 2.8%. The comparison of the other type of solar air heater is shown in Fig. 7 and it has a significant effect on improving its efficiency.

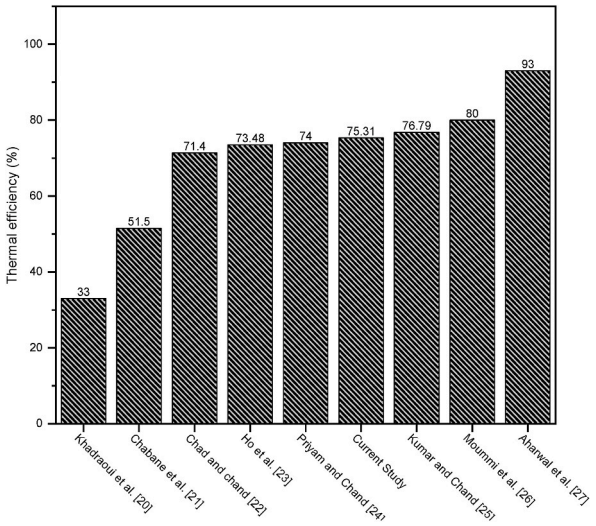

Fig. 7. Comparison of the sustainability index and solar intensity.

5. Conclusions

5.1. *Following conclusions are drawn on the basis of experimental observations and CFD analysis*

- The experimental investigation shows that the TSAH entrance air temperature ranges from 307 to 310 K.
- The CFD results shows a large temperature and pressure gradient within the duct, indicating that the pressure is higher in the input region than in the output region. The temperature of the absorber plate increases as solar radiation rises.
- Nusselt and Reynolds numbers are proportional. As P/D and e/D are decreased, the average Nusselt number rises.
- At a solar intensity between 630 and 1080 W/m^2, the thermal efficiency of TSAH with roughened absorber plate is 4.56–5.34% higher than that of TSAH with a smooth absorber plate. At 750 W/m^2 of solar intensity, thermal efficiency is maximum (75.31%).
- The CFD analysis found that the best inlet-to-outlet temperature difference was achieved with a V-shaped roughness with a rib. In addition, there is a decrease in pumping losses and an improvement in efficiency.

Author statement

Rahul Kumar: Conceptualization, Software. Sujit Kumar Verma: Methodology, Data curation, Writing- Original draft preparation. Naveen Kumar Gupta: Visualization, Investigation. Andres Armando Mendiburu Zevallos: Supervision. Abhishek Sharma: Software, Validation. Tabish Alam: Writing- Reviewing and Editing, Sayed M Eldin: Formal Analysis, Validation.

Declaration of competing interest

The authors declare that they have no known competing financial interests or personal relationships that could have appeared to influence the work reported in this paper.

Data availability

The authors do not have permission to share data.

Abbreviations

CFD	Computational fluid dynamics
SAH	Solar air heater
THPP	Thermal hydraulic performance parameter
TSAH	Triangular Solar air heater
FESEM	Field Emission Scanning Electron Microscope
EDS	Energy Dispersive X-Ray Spectroscopy

Appendix

The finite volume method is used in the ANSYS 14.5 fluid flow fluent.

$$\frac{\partial(\rho u_j)}{\partial x_j}=0$$

$$\frac{\partial(\rho u_i u_j)}{\partial x_j}=-\frac{\partial p}{\partial x_i}+\frac{\partial}{\partial x_j}\left[\mu\left(\frac{\partial u_i}{\partial x_j}+\frac{\partial u_j}{\partial x_i}\right)+\mu_t\left(\frac{\partial u_i}{\partial x_j}+\frac{\partial u_j}{\partial x_i}\right)\right]$$

$$\frac{\partial(\rho u_i T)}{\partial x_i}-\frac{\partial}{\partial x_j}\left[(\Gamma+\Gamma_t)\frac{\partial T}{\partial x_j}\right]=0$$

Since the flow within the triangular section is turbulent, the analysis is done using the *k*-ε model. The transport equations are used in the RNG, and the k-ε model is given below.

$$N_{u_r}=\frac{hD_h}{k}$$

$$h=\frac{Q_u}{A_p(T_p-T_f)}\ and\ Q_u=mC_p(T_o-T_i)$$

$$f_r=\frac{\left(\frac{\Delta P}{l}\right)D_h}{2\rho V^2}$$

$$R_e=\frac{\rho V D_h}{\mu}$$

$$THPP=\frac{N_{u_r}/N_{u_s}}{(f_r/f_s)^{1/3}}$$

$$N_{u_s}=0.023Re^{0.8}\ Pr^{0.4}$$

$$f_s=0.0791\ Re^{-0.25}$$

$$\frac{\partial(\rho k u_i)}{\partial x_i}=\frac{\partial}{\partial x_j}\left(\mu_{eff}\alpha_k\frac{\partial k}{\partial x_j}\right)+G_k-\varepsilon\rho$$

Uncertainty Analysis

Uncertainty analysis is a very useful method of analyzing the experimental results. Uncertainties in experimental measurement may arise as a result of test conditions, device usage, device standardization, and thermocouple connection points.

$$W_R=\left[\left(\frac{\partial R}{\partial x_1}w_1\right)^2+\left(\frac{\partial R}{\partial x_1}w_1\right)^2+\ldots+\left(\frac{\partial R}{\partial x_n}w_n\right)^2\right]^{1/2}$$

References

[1] G. Wang, L. Feng, M. Altanji, K. Sharma, K. Sooppy Nisar, S. khorasani, Proposing novel "L" shaped fin to boost the melting performance of a vertical PCM enclosure, Case Stud. Therm. Eng. (2021), https://doi.org/10.1016/j.csite.2021.101465.

[2] A.K. Pandey, R. Reji Kumar, B K, I.A. Laghari, M. Samykano, R. Kothari, A.M. Abusorrah, K. Sharma, V.V. Tyagi, Utilization of solar energy for wastewater treatment: challenges and progressive research trends, J. Environ. Manag. (2021), https://doi.org/10.1016/j.jenvman.2021.113300.

[3] S. Kumar, R.K. Das, K. Kulkarni, Comparative study of solar air heater (SAH) roughened with transverse ribs of NACA 0020 in forward and reverse direction, Case Stud. Therm. Eng. 34 (2022), 102015, https://doi.org/10.1016/j.csite.2022.102015.

[4] R. Kumar, S. Kumar Verma, Performance estimation of Triangular Solar air heater roughened absorber surface: an experimental and simulation modeling, Sustain. Energy Technol. Assessments 52 (2022), 102208, https://doi.org/10.1016/j.seta.2022.102208.

[5] G.K. Poongavanam, K. Panchabikesan, A.J.D. Leo, V. Ramalingam, Experimental investigation on heat transfer augmentation of solar air heater using shot blasted V-corrugated absorber plate, Renew. Energy 127 (2018) 213–229, https://doi.org/10.1016/j.renene.2018.04.056.

[6] A.K. Pandey, I. Ali Laghari, R. Reji Kumar, K. Chopra, M. Samykano, A.M. Abusorrah, K. Sharma, V.V. Tyagi, Energy, exergy, exergoeconomic and enviroeconomic (4-E) assessment of solar water heater with/without phase change material for building and other applications: a comprehensive review, Sustain. Energy Technol. Assessments (2021), https://doi.org/10.1016/j.seta.2021.101139.

[7] P.K. Jain, A. Lanjewar, Overview of V-RIB geometries in solar air heater and performance evaluation of a new V-RIB geometry, Renew. Energy 133 (2019) 77–90, https://doi.org/10.1016/j.renene.2018.10.001.

[8] A.E. Kabeel, M.H. Hamed, Z.M. Omara, A.W. Kandeal, Solar air heaters: design configurations, improvement methods and applications – a detailed review, Renew. Sustain. Energy Rev. 70 (2017) 1189–1206, https://doi.org/10.1016/j.rser.2016.12.021.

[9] John A. Duffie, William A. Beckman, Solar Engineering of Thermal Processes, fourth ed., 2013.
[10] N. Akhtar, S.C. Mullick, Approximate method for computation of glass cover temperature and top heat-loss coefficient of solar collectors with single glazing, Sol. Energy 66 (1999) 349–354, https://doi.org/10.1016/S0038-092X(99)00032-8.
[11] S.A. Klein, Calculation of flat-plate collector loss coefficients, Sol. Energy 17 (1975) 79, https://doi.org/10.1016/0038-092X(75)90020-1.
[12] K. Nidhul, S. Kumar, A.K. Yadav, S. Anish, Enhanced thermo-hydraulic performance in a V-ribbed triangular duct solar air heater: CFD and exergy analysis, Energy 200 (2020), 117448, https://doi.org/10.1016/j.energy.2020.117448.
[13] E.B. Wylie, V.L. Streeter, Fluid Transients, McGraw-Hill., New York, 1978.
[14] Numerical investigation of performance analysis of Triangular Solar air heater using Computational Fluid Dynamics (CFD) - IOPscience (2022). https://iopscience.iop.org/article/10.1088/1757-899X/1116/1/012047. (Accessed 13 December 2022).
[15] R. Kumar, S.K. Verma, M. Singh, Experimental investigation of nanomaterial doped in black paint coating on absorber for energy conversion applications, Mater. Today Proc. 44 (2021) 961–967, https://doi.org/10.1016/j.matpr.2020.11.006.
[16] R.W. Bliss, The derivations of several "Plate-efficiency factors" useful in the design of flat-plate solar heat collectors, Sol. Energy 3 (1959) 55–64, https://doi.org/10.1016/0038-092X(59)90006-4.
[17] S.A. Kalogirou, Solar Energy Engineering: Processes and Systems, Academic Press, 2013.
[18] T.K. Abdelkader, Y. Zhang, E.S. Gaballah, et al., Energy and exergy analysis of a flat-plate solar air heater coated with carbon nanotubes and cupric oxide nanoparticles embedded in black paint, J. Clean. Prod. (2019), 119501, https://doi.org/10.1016/j.jclepro.2019.119501.
[19] S.A. Klein, Calculation of the monthly-average transmittance-absorptance product, Sol. Energy 23 (1979) 547–551, https://doi.org/10.1016/0038-092X(79)90083-5.